Original Article

Available online at
www.heca-analitika.com/ljes

Leuser Journal of Environmental Studies

Vol. 1, No. 2, 2023

Exploring Geothermal Manifestations in Ie Jue, Indonesia: Enhancing Safety with Unmanned Aerial Vehicle

Aprianto Aprianto [1], Aga Maulana [1], Teuku Rizky Noviandy [1], Andi Lala [2], Muhammad Yusuf [3], Marwan Marwan [4], Razief Perucha Fauzie Afidh [1], Irvanizam Irvanizam [1], Nizamuddin Nizamuddin [1] and Ghazi Mauer Idroes [2,5,*]

[1] Department of Informatics, Faculty of Mathematics and Natural Sciences, Universitas Syiah Kuala, Banda Aceh 23111, Indonesia; apryanto178@gmail.com (A.A.); agamaulana@usk.ac.id (A.M.); trizkynoviandy@gmail.com (T.R.N.); razief@usk.ac.id (R.P.F.A.); irvanizam.zamanhuri@usk.ac.id; niz4muddin@unsyiah.ac.id (N.N.)
[2] School of Mathematics and Applied Sciences, Universitas Syiah Kuala, Banda Aceh 23111, Indonesia; andi_lala@usk.ac.id (A.L.); idroesghazi_k3@abulyatama.ac.id (G.M.I.)
[3] Department of Pharmacy, STIKES Assyifa Aceh, Banda Aceh 23242, Indonesia; iamyusufibrahim@gmail.com (M.Y.)
[4] Department of Geophysical Engineering, Faculty of Engineering, Universitas Syiah Kuala, Banda Aceh, 23111, Indonesia; marwan.geo@usk.ac.id (M.M.)
[5] Department of Occupational Health and Safety, Faculty of Health Sciences, Universitas Abulyatama, Aceh Besar 23372, Indonesia;

***** Correspondence: idroesghazi_k3@abulyatama.ac.id

Article History

Received 4 September 2023
Revised 4 October 2023
Accepted 18 October 2023
Available Online 23 October 2023

Keywords:
Surface temperature
Drone
FLIR
Satellite image

Abstract

Geothermal energy is a renewable resource derived from the Earth's interior that provides an environmentally friendly alternative. Indonesia is at the forefront of geothermal potential, possessing ample resources primarily concentrated in places like Sumatra. However, there is a requirement for greater exploitation of this potential. This research utilizes unmanned aerial vehicles (UAVs) and thermal imaging to detect geothermal indications in the Ie Jue region of Sumatra within the province of Aceh, Indonesia. The analysis focuses on three main manifestation locations using FLIR One thermal camera and water temperature gauges. The study leverages satellite imagery for comparative purposes. Temperature data highlights variations among distinct manifestations, underscoring the necessity for thorough exploration. Moreover, the study devises a secure pathway for researchers to access the site. This investigation contributes to comprehending geothermal activity and its possible role in sustainable energy and other domains.

1. Introduction

Geothermal energy is a renewable source that harnesses heat from the Earth's interior. It stands out as an environmentally friendly option, drawing its power from the Earth's heat reservoirs [1, 2]. Indonesia stands out among nations as the world's leading holder of abundant geothermal resources, possessing the highest potential in this domain [3]. Indonesia's geothermal capacity reaches approximately 28,617 MW, constituting nearly 40 percent of the global geothermal potential. Nonetheless, only a mere 4.5% of this capacity is currently utilized for generating electrical energy [4, 5].

In Indonesia, the geothermal potential peaks in Sumatra, with an estimated capacity of approximately 12,760 MW [6, 7]. Among the peaks within the Sumatra region, Seulawah Agam stands out as a mountain predicted to

hold a geothermal capacity of 275 MW. Unfortunately, this potential largely remains untapped [6]. Aceh, situated in Sumatra, is recognized for its geothermal reserves with significant developmental possibilities. The Jaboi geothermal site [8, 9] and Seulawah Agam [6, 7, 10] are two promising areas in Aceh for geothermal advancement. Numerous zones within Seulawah Agam exhibit potential for harnessing geothermal energy, including the Ie Brouk geothermal site [11] and the Ie Jue geothermal location [10, 12].

Geothermal manifestations offer advantages in the energy field and extend their benefits to other domains, including pharmaceuticals [13–16]. These manifestations involve releasing reservoir geothermal fluids to the surface through permeable zones or cracks. These manifestations can present in various forms, such as hot springs, warm springs, hot pools, geysers, and fumaroles. Fumaroles, in particular, denote the emission of hot steam through rock fissures, which condenses into water vapor (steam). Furthermore, this area holds the potential for conducting geothermal studies [17–20].

Unmanned Aerial Vehicles (UAVs) or drones are one of the technologies currently being researched for large-scale mapping [21–23]. Drones have several advantages over satellite imagery, including the ability to operate relatively rapidly and repeatedly, the ability to fly low to capture high-resolution photos, cheaper costs, a wider range of uses, and the absence of a pilot [24, 25]. Notably, drones can effectively address a common challenge in satellite imagery recording, which is the interference caused by factors like clouds and other disturbances during the recording process [26–30].

The primary aim of this study is to employ UAV technology to investigate and map the geothermal manifestations in the Ie Jue region of Aceh, Indonesia. By generating a detailed geothermal manifestation map, we seek to enhance our understanding of geothermal activity in this area and, at the same time, provide a valuable tool to improve exploration safety. This map not only helps identify hazardous areas and safe routes for geothermal researchers but also offers valuable insights into the various geothermal manifestations present.

2. Materials and Methods

2.1. Equipment and Software

The equipment employed in this investigation comprises a laptop, a DJI Phantom 4 Standard drone, FLIR One Gen 2, GPS Map 62s, Milwaukee Mi306, and an Android smartphone (Xiaomi Redmi 3). The corresponding software tools encompass Avenza Maps, SAS Planet, FLIR One, ArcMap version 10.5, and ArcScene version 10.5. These technological resources are highly advantageous for accessing remote survey areas with logistical challenges. They greatly aid research by pinpointing temperature variations during exploration.

2.2. Determining Coordinate Location

The GPS Map 62s was employed to ascertain the coordinate position, aligning with previous investigations where the study's location coordinates and altitude data were gathered at the identical site, with a slight modification [7]. Three sample locations are identified as IJ1, IJ2, and IJ3. The precise coordinates for these investigation sites are outlined in Table 1.

2.3. Retrieval of FLIR Images

Images and temperatures were acquired using the FLIR One Gen 2 Infrared Thermal camera linked to the Xiaomi Redmi 3 smartphone. Both of these devices were mounted on the DJI Phantom 4 Standard Drone for the data collection. The gathered images and temperature readings pinpoint the locations of geothermal phenomena in the Ie Jue area. Drones offer exceptional functionality as they can access remote and inaccessible areas, making capturing images through FLIR One considerably more convenient from various locations.

2.4. Retrieval of Temperature Data

This study necessitates the inclusion of three distinct temperature datasets: the temperature of geothermal manifestations acquired through the FLIR One camera, water temperature data, and temperature data derived from satellite imagery. Regarding water temperature, measurements were directly taken at the research site using the Milwaukee Mi306 Conductivity tool. Collecting water temperature data involved three separate instances to ensure a comprehensive dataset for thorough analysis. As for satellite imagery, temperature data is extracted from Landsat 8 satellite scans. Landsat 8 satellite images were processed using ArcMap to extract the corresponding Land Surface Temperature values.

Table 1. Coordinate Locations of Research Survey Area.

Sample Location	Coordinates		Elevation (m)
	N	E	
IJ1	5°30′24.62″	95°37′43.98″	252
IJ2	5°30′24.35″	95°37′44.40″	254
IJ3	5°30′24.12″	95°37′45.15″	254

Figure 1. Geothermal manifestation in Ie Jue.

Table 2. Results of FLIR image temperature data analysis.

	IJ1 (°C)	IJ2 (°C)	IJ3 (°C)
Mean	72.8	74.5	83.6
Maximum	74.4	75.8	85.9
Minimum	71.9	73.0	79.0

2.5. Temperature Data

The temperature data extracted from the FLIR One image is compared with the temperature data collected from Landsat 8 satellite images to evaluate the effectiveness of both FLIR One and Landsat 8 satellite imagery in gauging the surface temperature of the Ie Jue geothermal manifestation. This comparative analysis is a benchmark for subsequent research endeavors at the Ie Jue site.

2.6. Creating Ie Jue Geothermal Manifestation Map Layout

The study utilizes the ArcMap tool to compile research findings to create maps. The resulting map depicts a secure route and the precise coordinates of the geothermal manifestation. The Avenza Map program navigates the safe route, enabling convenient access to and from the Ie Jue region.

3. Results and Discussion

3.1. Geothermal Manifestation

Figure 1 shows the geothermal manifestation in Ie Jue. IJ1 manifestation is a hot water flow emanating from a single point within a hot spring and cascading outward. In contrast, the IJ2 manifestation takes the form of a hot water pool with a comparatively modest spring discharge. Simultaneously, the IJ3 manifestation is a simmering water basin where bubbles surge to the surface. This distinct presentation underscores the varying characteristics inherent in each scrutinized manifestation.

3.2. Analysis of FLIR Image Temperature Data

Table 2 provides insight into the FLIR temperature analysis results, revealing distinct average values at each designated coordinate location. Specifically, the IJ1 coordinate location exhibits an average FLIR image temperature value of 72.8 °C, akin to the IJ2 coordinate location's reading. The comprehensive average temperature for the FLIR image stands at 74.5 °C. Notably, the IJ3 coordinate location records a substantially higher average FLIR image temperature value of 83.6 °C.

The FLIR image data analysis reveals the dataset's highest and lowest temperature values. Notably, the IJ3 coordinate location registers the highest temperature value at 74.4 °C, while the lowest temperature reading of 71.9 °C is observed at the IJ1 coordinate location.

The FLIR image employs a color-coded scheme to delineate temperatures across various locations, encompassing the manifestation site and its immediate vicinity. Figure 2 visually captures these temperature distinctions within the FLIR image. The thermal palette provided by FLIR One is instrumental in interpreting these color variations. It becomes evident that the FLIR One image employs a spectrum of colors to differentiate between the manifestation area and its surroundings. Colors can be interpreted based on the thermal palette. The manifestation site is depicted in white, whereas the surrounding area ranges from bluish-orange to blackish-blue. Different features are distinguishable, such as rocks adjacent to the manifestation site (appearing as blue-black regions) and damp soil above the hot spring (marked by bluish-orange shades). Notably, locations transitioning from orange to white outside the manifestation site are potential zones for future manifestations.

3.3. Analysis of Water Temperature Data

After acquiring water temperature data, a comprehensive analysis identifies each dataset's highest and lowest temperature values. The outcome is the

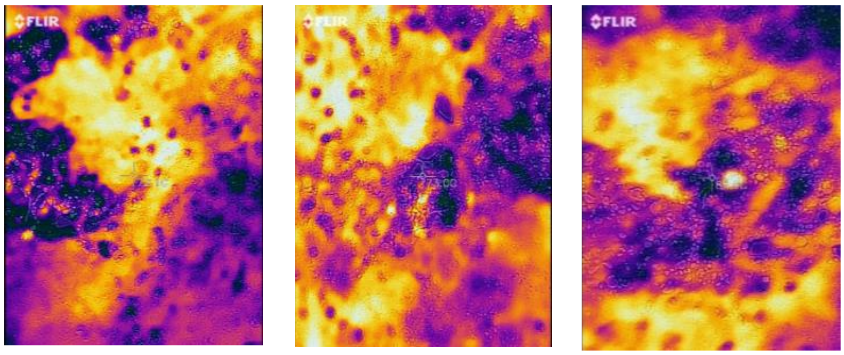

(a) (b) (c)

Figure 2. FLIR One image results for (a) IJ1, (b) IJ2, and (c) IJ3.

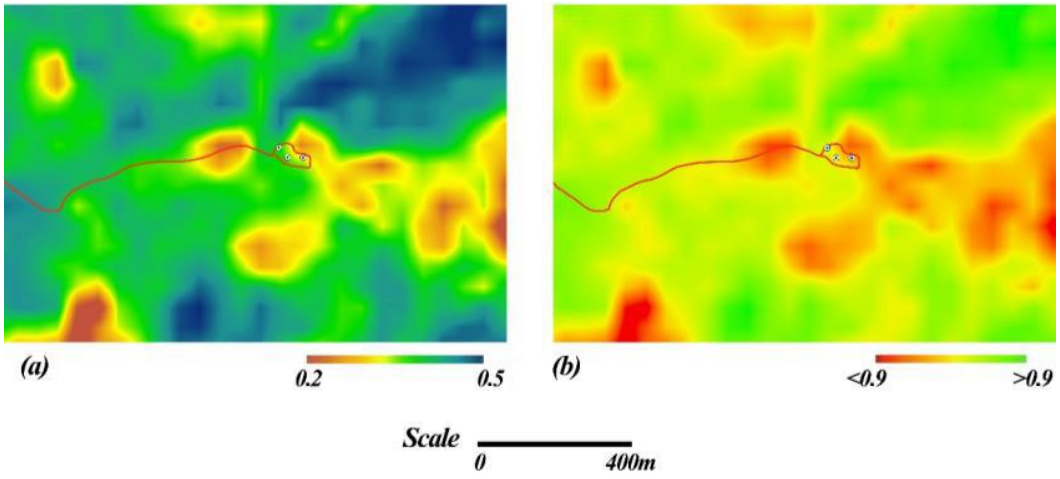

Figure 3. Analysis of (a) NDVI and (b) Emissivity of Landsat 8 Satellite Imagery

Table 3. Water temperature data analysis results

	IJ1 (°C)	IJ2 (°C)	IJ3 (°C)
Mean	90.09	90.32	90.83
Maximum	90.12	90.34	90.85
Minimum	90.07	90.29	90.82

generation of average values for each data set, enabling the detection of differences.

Based on the findings in Table 3, the data analysis yields distinct average values for the respective tests (IJ1, IJ2, IJ3): 90.09 °C, 90.32 °C, and 90.83 °C. The highest temperature readings are recorded at IJ1 (90.12 °C), IJ2 (90.34 °C), and IJ3 (90.85 °C), while the lowest temperatures are noted at IJ1 (90.07 °C), IJ2 (90.29 °C), and IJ3 (90.82 °C).

The disparity in water temperature values among geothermal manifestations is attributed to the distinctive characteristics of each site's hot water. The temperature data analysis also unveils that the highest average temperature value is found at the IJ3 coordinate location (90.83 °C), surpassing the averages at IJ1 and IJ2. Conversely, the lowest average temperature is observed at the IJ1 coordinate location (90.09 °C), lower than the averages at IJ2 and IJ3.

3.4. Analysis of Satellite Image Temperature Data

The satellite image harnessed for this study originates from Landsat 8 Level 1 TP, equipped with two sensors: the Operational Land Imager (OLI) and the Thermal Infrared Sensor (TIRS). These sensors provide spatial resolutions of 30 meters for Visual Near Infra-Red (VNIR), Near Infra-Red (NIR), and Short-Wave Infrared (SWIR) bands, 100 meters for Thermal bands, and 15 meters for the panchromatic band. Landsat 8 features five VNIR bands (bands 1 - 5), two SWIR bands (bands 6 and 7), one panchromatic band (band 8), one cirrus band (band 9), and two Thermal Infrared (TIR) bands (bands 10 and 11). Given the low resolution of satellite data, only three data pixels represent the small geothermal manifestation areas (50 x 50 m) for the Thermal band.

Following satellite image processing, normalized difference vegetation index (NDVI) and emissivity images are derived, as shown in Figure 3. NDVI (Normalized Difference Vegetation Index) is a remote sensing metric used to assess vegetation health and density by comparing near-infrared and red-light measurements, with higher values indicating healthier vegetation. Emissivity, on the other hand, measures an object's efficiency in emitting thermal infrared radiation.

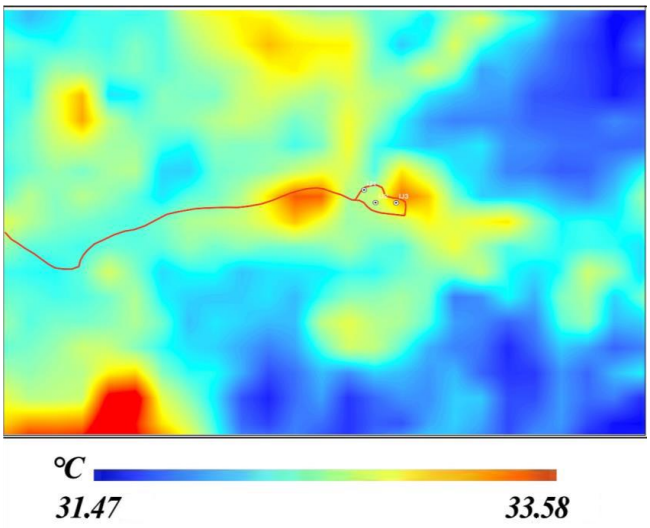

Figure 4. Image result of land surface temperature.

Emissivity is crucial for understanding thermal properties and is often used in applications like land surface temperature estimation and environmental monitoring. NDVI data exhibits contrast variations between surrounding areas, with values spanning 0.2 to 0.5. Emissivity data, calculated from NDVI, follows a similar pattern, indicating low emissivity (<0.9) near manifestation locations. This lower emissivity indicates a response to a diminished ratio of radiation energy emitted by the ground surface.

Further processing leads to deriving Land Surface Temperature (LST) values from NDVI and emissivity. The LST values range between 31.47 °C and 33.58 °C, originating from processing LST values in bands 10 and 11. These values are then averaged to ascertain the average temperature at the research site, as depicted in Figure 4. The land surface temperature image with distinct colors demarcates areas of high and low-temperature values. Notably, the image indicates the highest temperature as 33.58 °C, depicted in orange, while the lowest temperature is 31.47 °C, represented by a blue area. Coordinate locations pertinent to the study are integrated into the land surface temperature image, facilitating temperature identification through identification tools.

The Land Surface Temperature (LST) values extracted from the image reveal that the temperature at the IJ1 coordinate location is measured at 32.41 °C, while the IJ2 coordinate location also exhibits a temperature of 32.41 °C. Conversely, the IJ3 coordinate location records a higher temperature of 32.99 °C. It becomes apparent that the lowest surface temperatures are found at the IJ1 and IJ2 coordinate locations, both registering 32.4 °C. In contrast, the highest surface temperature of 32.9 °C is observed at the IJ3 coordinate location. Notably, areas outside the geothermal manifestation site exhibit temperatures around 31.9 °C.

3.5. Temperature Comparison

The initial comparison of temperature data encompasses two distinct datasets. The first dataset comprises water temperature data derived from this study, while the second dataset involves FLIR image temperature data obtained through drone-based testing utilizing FLIR thermal cameras. The water temperature data represents the average temperature at each coordinate location, while the FLIR image temperature data is based on average temperature values at these coordinates.

The relatively minor contrast between water and FLIR temperature data is illustrated in Figure 5. Specifically, at the IJ1, IJ2, and IJ3 coordinate locations, water temperature data registers 90.09 °C, 90.32 °C, and 90.83 °C, respectively. In contrast, FLIR temperature readings for the same locations are 72.8 °C, 74.5 °C, and 83.6 °C.

3.6. Ie Jue Geothermal Manifestation Map Layout

The layout map of Ie Jue geothermal manifestations undergoing ArcMap software processing is depicted, where a structured layout is created within ArcMap by inputting location coordinates and security path information (Figure 6). The map is presented with a scale of 1 centimeter to 40 meters. Research sites are highlighted with red marks on the index map. Furthermore, location coordinates are denoted by white circular symbols, each with a diameter of 15.00 units, and accompanied by labels corresponding to the sample locations.

This layout map clearly illustrates the secure path, indicating that the route to the research location or the coordinates of the thermal features avoids traversing

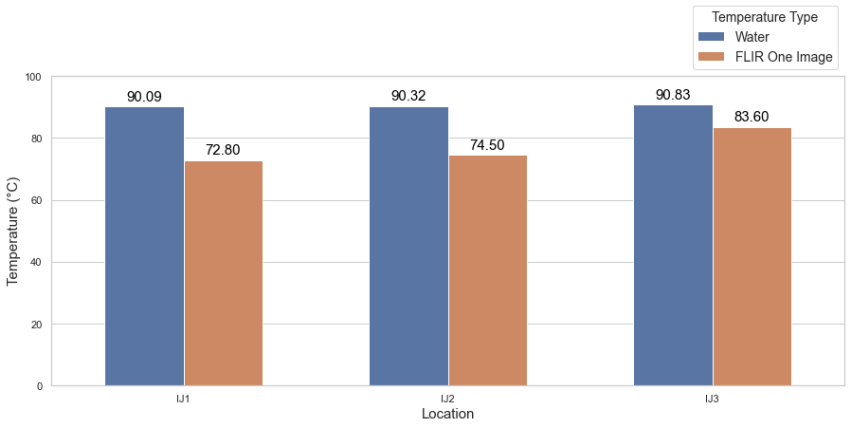

Figure 5. Image result of land surface temperature.

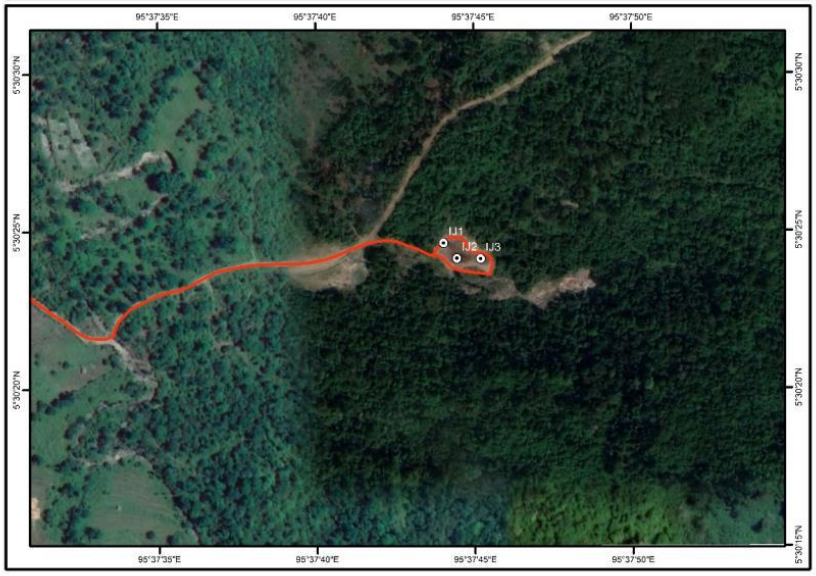

Figure 6. Ie Jue geothermal manifestation map layout.

areas populated with shrubs, hot springs, or other thermal elements. As this path eliminates potential hazards for researchers during their investigations, it represents the safest course of travel to reach the research location.

4. Conclusions

This study successfully achieved its objective of investigating geothermal manifestations in the Ie Jue region of Aceh, Indonesia using UAV technology and generating a comprehensive geothermal manifestation map. The mapped pathways created in the process not only serve to identify and map the various geothermal manifestations in the area but also enhance exploration safety. The resulting manifestation map contributes significantly to our understanding of geothermal activity in the region and provides a valuable tool for researchers and professionals involved in geothermal studies. By integrating UAV technology and thermal imaging, this study offers valuable insights into the distribution and nature of geothermal manifestations while prioritizing safety in exploration endeavors. It demonstrates the effective utilization of drones equipped with FLIR thermal cameras for enhancing safety and efficiency in geothermal exploration, thereby advancing the field and reducing research duration. These findings underscore the potential of drone and FLIR One technology in advancing geothermal exploration practices, aligning with the study's overarching aims.

Author Contributions: Conceptualization, A.A., A.M., T.R.N., A.L., and G.M.I.; methodology, A.A., M.M., R.P.F.A., I.I., N.N. and G.M.I.; software, A.A., A.L., and M.Y.; validation, M.M., I.I., N.N., and G.M.I.; formal analysis, A.A., A.M., T.R.N., and R.P.F.A.; investigation, A.A., A.L. and M.Y.; resources, I.I., N.N., and G.M.I.; data curation, M.M., N.N. and G.M.I.; writing—original draft preparation, A.A., A.M. and T.R.N.; writing—review and editing, I.I., N.N. and G.M.I.; visualization, A.L., M.Y., and M.M.; supervision, I.I., N.N. and G.M.I.; project administration, G.M.I. All authors have read and agreed to the published version of the manuscript.

Funding: This study does not receive external funding.

Ethical Clearance: Not applicable,

Informed Consent Statement: Not applicable.

Data Availability Statement: The data is available upon reasonable request to the corresponding author.

Acknowledgments: The authors gratefully acknowledge their respective institutions and universities for their support and resources.

Conflicts of Interest: All the authors declare that there are no conflicts of interest.

References

1. Stober, I., and Bucher, K. (2013). Geothermal energy, *Germany: Springer-Verlag Berlin Heidelberg. Doi*, Vol. 10, 973–978.
2. Bashir, M. A., Dengfeng, Z., Shahzadi, I., and Bashir, M. F. (2023). Does geothermal energy and natural resources affect environmental sustainability? Evidence in the lens of sustainable development, *Environmental Science and Pollution Research*, Vol. 30, No. 8, 21769–21780.
3. Fan, K., and Nam, S. (2018). Accelerating geothermal development in Indonesia: A case study in the underutilization of geothermal energy, *Consilience*, No. 19, 103–129.
4. Mohammadzadeh Bina, S., Jalilinasrabady, S., Fujii, H., and Pambudi, N. A. (2018). Classification of geothermal resources in Indonesia by applying exergy concept, *Renewable and Sustainable Energy Reviews*, Vol. 93, 499–506. doi:10.1016/j.rser.2018.05.018.
5. Idroes, G. M., Syahnur, S., Majid, M. S. A., Idroes, R., Kusumo, F., and Hardi, I. (2023). Unveiling the Carbon Footprint: Biomass vs. Geothermal Energy in Indonesia, *Ekonomikalia Journal of Economics*, Vol. 1, No. 1, 10–18. doi:10.60084/eje.v1i1.47.
6. Marwan, M., Yanis, M., Nugraha, G. S., Zainal, M., Arahman, N., Idroes, R., Dharma, D. B., Saputra, D., and Gunawan, P. (2021). Mapping of Fault and Hydrothermal System beneath the Seulawah Volcano Inferred from a Magnetotellurics Structure, *Energies*, Vol. 14, No. 19, 6091. doi:10.3390/en14196091.
7. Idroes, R., Yusuf, M., Saiful, S., Alatas, M., Subhan, S., Lala, A., Muslem, M., Suhendra, R., Idroes, G. M., Marwan, M., and Mahlia, T. M. I. (2019). Geochemistry Exploration and Geothermometry Application in the North Zone of Seulawah Agam, Aceh Besar District, Indonesia, *Energies*, Vol. 12, No. 23, 4442. doi:10.3390/en12234442.
8. Idroes, R., Marwan, M., Yusuf, M., Muslem, M., and Helwani, Z. (2021). Geochemical Investigation on Jaboi Manifestation, Jaboi Volcano, Sabang, Indonesia, *International Journal of GEOMATE*, Vol. 20, No. 82. doi:10.21660/2021.82.j2114.
9. Idroes, R., Yusuf, M., Lala, A., Muslem, M., Mahmudi, M., Suhendra, R., Idroes, G. M., Abakar, M., Helwani, Z., and Mahlia, T. M. I. (2020). Geochemistry Exploration and Geothermometry Application in Jaboi Manifestation, Jaboi Volcano, Sabang, Indonesia, *Geofluids*.
10. Bahri, R. A., Noviandy, T. R., Suhendra, R., Idroes, G. M., Yanis, M., Yandri, E., Nizamuddin, N., and Irvanizam, I. (2023). Utilization of Drone with Thermal Camera in Mapping Digital Elevation Model for Ie Seu'um Geothermal Manifestation Exploration Security, *Leuser Journal of Environmental Studies*, Vol. 1, No. 1, 25–33. doi:10.60084/ljes.v1i1.40.
11. Idroes, R., Yusuf, M., Alatas, M., Subhan, Lala, A., Muslem, Suhendra, R., Idroes, G. M., Suhendrayatna, Marwan, and Riza, M. (2019). Geochemistry of warm springs in the Ie Brôuk hydrothermal areas at Aceh Besar district, *IOP Conference Series: Materials Science and Engineering*, Vol. 523, 012010. doi:10.1088/1757-899X/523/1/012010.
12. Idroes, R., Yusuf, M., Alatas, M., Lala, A., Suhendra, R., and Idroes, G. M. (2019). Geochemistry of Sulphate spring in the Ie Jue geothermal areas at Aceh Besar district, Indonesia, *IOP Conference Series: Materials Science and Engineering* (Vol. 523), IOP Publishing, 12012.
13. Azhari, S., Ningsih, D. S., Nuraskin, C. A., Karma, T., Muslem, Idroes, G. M., Suhendra, R., Tallei, T. E., Rahimah, S., Khairan, and Idroes, R. (2021). Identification of Geothermal and Non-Geothermal Laban Plant (Vitex Pinnata) With a Combination of Infrared Spectroscopy – Principal Component Analysis Methods, *Proceedings of the 1st Aceh International Dental Meeting (AIDEM 2019), Oral Health International Conference On Art, Nature And Material Science Development 2019*, Atlantis Press, Paris, France. doi:10.2991/ahsr.k.210201.019.
14. Maulana, A., Noviandy, T. R., Idroes, R., Sasmita, N. R., Suhendra, R., and Irvanizam, I. (2020). Prediction of Kovats Retention Indices for Flavor and Fragrance Compounds using Artificial Neural Network, *2020 International Conference on Electrical Engineering and Informatics (ICELTICs)*, IEEE, Banda Aceh.
15. Maulydia, N. B., Khairan, K., and Noviandy, T. R. (2023). Prediction of Pharmacokinetic Parameters from Ethanolic Extract Mane Leaves (Vitex pinnata L.) in Geothermal Manifestation of Seulawah Agam Ie-Seu'um, Aceh, *Malacca Pharmaceutics*, Vol. 1, No. 1, 16–21. doi:10.60084/mp.v1i1.33.
16. Fakri, F., Harahap, S. P., Muhni, A., Khairan, K., Hewindati, Y. T., and Idroes, G. M. (2023). Antimicrobial Properties of Medicinal Plants in the Lower Area of Ie Seu-um Geothermal Outflow, Indonesia, *Malacca Pharmaceutics*, Vol. 1, No. 2, 55–61. doi:10.60084/mp.v1i2.44.
17. Stelling, P., Shevenell, L., Hinz, N., Coolbaugh, M., Melosh, G., and Cumming, W. (2016). Geothermal systems in volcanic arcs: Volcanic characteristics and surface manifestations as indicators of geothermal potential and favorability worldwide, *Journal of Volcanology and Geothermal Research*, Vol. 324, 57–72. doi:10.1016/j.jvolgeores.2016.05.018.
18. Ayu, D., Arifin, Y. I., Zainuri, A., Manyoe, I. N., and Jahja, M. (2023). Geology and Geophysics of Talumopatu Geothermal Manifestation Area of Mootilango District, Gorontalo Regency, Indonesia, *E3S Web of Conferences* (Vol. 400), EDP Sciences, 1013.
19. Farid, M., Andeska, D. O., and Hadi, A. I. (2023). Stratification characteristics of subsurface rock structure geothermal manifestations at Telaga Tujuh Warna Bukit Daun, Bengkulu, Indonesia using magnetic methods, *Journal of Physics: Conference Series* (Vol. 2498), IOP Publishing, 12008.
20. Putri, D. R., N. Ismail, R. Idroes, M. Marwan, S. Rizal, Abdulmadjid, S. N., Idroes, G. M., Noviandy, T. R., A. Lala, M. Yusuf, M. Muslem, R. Suhendra, M. Yanis, and D. B. Dharma. (2023). Geochemical Investigation of Hot Springs in the Bur Ni Geureudong Geothermal Prospect Area, Aceh-Indonesia, *RASAYAN Journal of Chemistry*, Vol. 16, No. 03, 1826–1834. doi:10.31788/RJC.2023.1638430.
21. Gupta, L., Jain, R., and Vaszkun, G. (2015). Survey of important issues in UAV communication networks, *IEEE Communications Surveys & Tutorials*, Vol. 18, No. 2, 1123–1152.
22. Studiawan, H., Grispos, G., and Choo, K.-K. R. (2023). Unmanned Aerial Vehicle (UAV) Forensics: The Good, The Bad, and the Unaddressed, *Computers & Security*, 103340.
23. Shahmoradi, J., Talebi, E., Roghanchi, P., and Hassanalian, M. (2020). A comprehensive review of applications of drone technology in the mining industry, *Drones*, Vol. 4, No. 3, 34.
24. Al-Dosari, K., Hunaiti, Z., and Balachandran, W. (2023). A review of civilian drones systems, applications, benefits, safety, and security challenges, *The Effect of Information Technology on Business and Marketing Intelligence Systems*, 793–812.
25. Emimi, M., Khaleel, M., and Alkrash, A. (2023). The current opportunities and challenges in drone technology, *International Journal of Electrical Engineering and Sustainability (IJEES)*, 74–89.

26. Shofiyanti, R. (2011). Teknologi Pesawat Tanpa Awak Untuk Pemetaan Dan Pemantauan Tanaman Dan Lahan Pertanian, *Jurnal Informatika Pertanian*, Vol. 20, No. 2, 58–64.

27. Marwan, Idroes, R., Yanis, M., Idroes, G. M., and Syahriza. (2021). A low-cost UAV based application for identify and mapping a geothermal feature in ie jue manifestation, Seulawah Volcano, Indonesia, *GEOMATE Journal*, Vol. 20, No. 80, 135–142.

28. Marwan, Noviandy, T. R., Maulana, A., Suhendra, R., Yusuf, M., Lala, A., Idroes, G. M., Muslem, Mahmudi, and Idroes, R. (2021). Utilization of unmanned aerial vehicles in geothermal exploration: A review, *IOP Conference Series: Materials Science and Engineering* (Vol. 1087), IOP Publishing, 12072.

29. Hardjono, T., Lipton, A., and Pentland, A. (2020). Toward an Interoperability Architecture for Blockchain Autonomous Systems, *IEEE Transactions on Engineering Management*, Vol. 67, No. 4, 1298–1309. doi:10.1109/TEM.2019.2920154.

30. Idroes, G. M., Maulana, A., Suhendra, R., Lala, A., Karma, T., Kusumo, F., Hewindati, Y. T., and Noviandy, T. R. (2023). TeutongNet: A Fine-Tuned Deep Learning Model for Improved Forest Fire Detection, *Leuser Journal of Environmental Studies*, Vol. 1, No. 1, 1–8. doi:10.60084/ljes.v1i1.42.